논문 13-38A-12-03

한국통신학회논문지(J-KICS) '13-12 Vol.38A No.12
http://dx.doi.org/10.7840/kics.2013.38A.12.998

Equalized Net Diffusion (END) for the Preservation of Fine Structures in PDE-based Image Restoration

Youngjoon Cha◆, Seongjai Kim*

ABSTRACT

The article is concerned with a mathematical modeling which can improve performances of PDE-based restoration models. Most PDE-based restoration models tend to lose fine structures due to certain degrees of nonphysical dissipation. Sources of such an undesirable dissipation are analyzed for total variation-based restoration models. Based on the analysis, the so-called equalized net diffusion (END) modeling is suggested in order for PDE-based restoration models to significantly reduce nonphysical dissipation. It has been numerically verified that the END-incorporated models can preserve and recover fine structures satisfactorily, outperforming the basic models for both quality and efficiency. Various numerical examples are shown to demonstrate effectiveness of the END modeling.

Key Words : Fine structures, nonphysical dissipation, total variation (TV) model, non-convex (NC) model, equalized net diffusion (END).

Ⅰ. INTRODUCTION

For diverse image-related applications, image restoration is an important image processing (IP) step and is often necessary as a pre-processing for other imaging tasks such as segmentation and compression. Thus image restoration has occupied a peculiar position in IP, computer graphics, and their applications[2,13,19,20,21,24,27].

There have been various partial differential equation (PDE)-based restoration models such as the Perona-Malik model[25], the total variation (TV) model[18,26], and color restoration models[3,10,15,17,28]. These PDE-based models have been extensively studied to answer fundamental questions in image restoration and have allowed researchers and practitioners not only to introduce new mathematical models but also to improve traditional algorithms[1,4,9,22,30].

However, most PDE-based restoration models and their numerical realizations show a common drawback: *loss of fine structures*. Such an undesirable loss is due to an excessive numerical dissipation introduced particularly on regions where the image content changes rapidly such as on edges and textures. Thus the reduction of nonphysical dissipation becomes an interesting problem in image restoration, requiring challenges and innovative ideas. Although advanced models have been recently suggested for the preservation of fine structures[19,23], more effective strategies have yet to be developed.

In this article, we will first analyze sources of nonphysical dissipation for popular PDE-based restoration models. Based on the analysis, we will study the so-called equalized net diffusion (END) modeling for PDE-based restoration models, first introduced in[14]. Here we will study mathematical

※ The work of the first author was supported by the National Research Foundation of Korea(NRF) grant funded by the Korea government(MEST) (No. 20110179). The work of the second author was supported in part by the NSF grant DMS-1228337.

◆ First Author : Department of Applied Mathematics, Sejong University, Gunja-Dong 98, Seoul 143-747, Korea, yjcha@sejong.ac.kr

* Department of Mathematics and Statistics, Mississippi State University, Mississippi State, MS 39762-5921, USA, skim@math.msstate.edu

논문번호 : KICS2013-11-503, 접수일자 : 2013년 11월 21일, 심사일자 : 2013년 12월 2일, 최종논문접수일자 : 2013년 12월 9일

properties of the END in detail and suggest a heuristic method for parameter choices. It has been numerically verified that with the new parameters, the END modeling can reduce nonphysical dissipation significantly and more effectively for most of natural images we have tested.

The article is organized as follows. In the next section, we review TV-based models along with recent studies for the reduction of nonphysical dissipation. Section III analyzes sources of nonphysical dissipation for PDE-based models: nonphysical dissipation occurs more excessively at pixels where the diffusion term evaluates larger in modulus. In Section IV, we introduce the END modeling which tries to equalize the net diffusion over a wide range of image frequencies. In the same section, a linearized numerical procedure is suggested for an efficient computation of END incorporated restoration models. Section V discusses a strategy for the choice of algorithm parameters introduced for the END modeling. In Section VI, we present numerical results to show effectiveness of the END modeling applied to two basic TV based models. The last section summarizes our experiments.

Ⅱ. PRELIMINARIES

2.1 Total variation (TV)-based models

Let f be the observed image of the form

$$f = u + v, \tag{1}$$

where u is a desired image and v denotes noise or the residual. A common mathematical denoising technique is to minimize the total variation (TV):

$$u = \arg\min_{u \in BV(\Omega)} \left\{ |u|_{BV} + \frac{\lambda}{2} \|f-u\|^2 \right\}, \tag{2}$$

where Ω is the image domain, λ is a nonnegative constraint constant, $\|\cdot\|$ denotes the L^2-norm, and $|\cdot|_{BV}$ is the bounded variation (BV) seminorm defined as

$$|u|_{BV} = \int_{\Omega} |\nabla u| \, d\mathbf{x}.$$

Apply the variational calculus [29, x3.3] to transform the minimization problem (2) into an equivalent differential equation, called the Euler-Lagrange equation of (2):

$$-\nabla \cdot \left(\frac{\nabla u}{|\nabla u|} \right) = \lambda (f-u). \tag{3}$$

Note that the restored image becomes closer to f as λ grows. For a convenient numerical simulation of (3), one may parameterize the energy descent direction by an artificial time t. Then the resulting equation reads the (evolutionary) TV model:

$$\frac{\partial u}{\partial t} - \nabla \cdot \left(\frac{\nabla u}{|\nabla u|} \right) = \lambda (f-u), \quad \text{(TV)} \tag{4}$$

where the no-flux boundary condition can be adopted, for simplicity, and $u(\cdot, t=0) = f$.

In the literature, the constraint parameter λ is often set as a constant, as suggested by Rudin-Osher-Fatemi[26]. In order to find the parameter, the authors merely multiplied (4) by $(f-u)$ and averaged the resulting equation over the whole image domain. Then, for its steady state,

$$\lambda = -\frac{1}{\sigma^2} \frac{1}{|\Omega|} \int_{\Omega} (f-u)\kappa(u) \, d\mathbf{x}. \tag{5}$$

where σ^2 is the noise variance.

Although the TV model pertains certain attractive mathematical properties in image restoration, its numerical realization may introduce a great deal of numerical dissipation particularly near fine structures. It is also known that the TV model tends to transform the image into a collection of locally constant portions, which is called the staircasing. As an antistaircasing approach, Marquina and Osher[18] introduced the *improved total variation* (ITV) model

$$\frac{\partial u}{\partial t} - |\nabla u| \nabla \cdot \left(\frac{\nabla u}{|\nabla u|} \right) = \lambda |\nabla u| (f-u). \quad \text{(ITV)} \tag{6}$$

The ITV model can be derived by scaling the stationary TV model (3) by a factor of $|\nabla u|$ and then introducing the time parameterization. Note that since $|\nabla u|$ vanishes only in flat regions, the steady

states of both TV and ITV models are analytically the same. The scaling can suppress the staircasing effectively, as claimed in [24, §11.3].

In order to prevent the denominator $|\nabla u|$ in (4) and (6) from approaching zero, it can be approximated as $|\nabla u| \approx |\nabla^{\varepsilon} u| := \sqrt{u_x^2 + u_y^2 + \varepsilon^2}$, for some $\varepsilon > 0$ small. As shown in [15], [16], such regularization can introduce larger nonphysical dissipation to destroy fine structures. To reduce the nonphysical dissipation, one may consider the following non-convex (NC) model:

$$\frac{\partial u}{\partial t} - |\nabla^{\varepsilon} u|^{1+\omega} \nabla \cdot \left(\frac{\nabla u}{|\nabla^{\varepsilon} u|^{1+\omega}} \right) = \beta(f-u), \quad \text{(NC)} \tag{7}$$

where $\omega \in [0,1)$ and $\beta = \beta(\mathbf{x},t) \geq 0$. See [15], [16] for effective strategies for the choice of ω and β, a non-standard numerical procedure, and its stability analysis. The NC model shares the same diffusion part as the ITV model when $\omega = 0$. As numerically verified in Section VI below, the NC model can preserve fine structures better than the ITV model. A variant of the NC model has been successfully applied as an edge-forming method for image zooming of arbitrary magnification factors[6,7].

Remark. The divergence term in (7), $-\nabla \cdot \left(\frac{\nabla u}{|\nabla^{\varepsilon} u|^{1+\omega}} \right)$, is corresponding to the following minimization

$$\min_{u} \int_{\Omega} |\nabla^{\varepsilon} u|^{1-\omega} d\mathbf{x},$$

of which the object is not convex for $\omega > 0$. (The model (7) has been named from the non-convexity.) It should be noticed that the NC model has a close relationship with the Perona-Malik model[25].

2.2. Recent studies for the reduction of nonphysical dissipation

For the TV-based image restoration, the staircasing effect is now well understood and relatively easy to handle compared with nonphysical dissipation. Here we review briefly two recent studies for the reduction of nonphysical dissipation[19,23].

As Meyer[19] analyzed, the L^2-norm applied to the residual $(f-u)$ in the TV model (4) is not sensitive enough to distinguish the noise from textures. As a consequence, the residual can easily contain not only the noise but also fine structures and therefore the restored image u turns out to be erroneous and blurry. To reduce the blur associated with the TV model, Meyer suggested the following modified variational problem:

$$u = \arg\min_{u \in BV(\Omega)} \left(|u|_{BV} + \lambda \|f-u\|_{*} \right), \tag{8}$$

where $\|\cdot\|_{*}$ denotes the norm in the Besov space $B_{\infty}^{-1,\infty}$; see [19, §1.13-1.15] for details. It has been observed that the Besov norm is able to distinguish between different textures; however, the model (7) is difficult to minimize using the Euler-Lagrange equation approach.

On the other hand, Osher et al.[23] recently suggested an iterative refinement procedure:

• *Initialize*: $u_0 = e_0 = 0$.

• *For* $k = 1,2,\cdots$; compute u_k as the minimizer of the following model

$$u_k = \arg\min_{u \in BV(\Omega)} \left(|u|_{BV} + \frac{\lambda}{2} \|f + e_{k-1} - u\|^2 \right) \tag{9}$$

and update

$$e_k = e_{k-1} + f - u_k. \tag{10}$$

The authors have proved that u_k converges monotonically in L^2 to f, the noisy image, as $k \to \infty$. The mathematical analysis can be interpreted *intuitively* as follows: Wherever the residual is nonzero, the residual is incorporated, as a source, into the constraint term in (9) for the computation of a new minimizer u_k and therefore the minimization problem can result in the new minimizer nearer to f than previous iterates. However, it is not necessarily beneficial for a denoising algorithm to have such a property (convergence to f), because the iterates u_k can get noisier as k grows. The iterative refinement may

restore not only fine structures but also the noise[23].

Ⅲ. DISSIPATION ANALYSIS

This section analyzes sources of excessive nonphysical dissipation, in particular near fine structures, for PDE-based restoration models. We will momentarily assume that the given image f involves no noise, i.e., $u(t=0) \equiv f$ and $v(t=0) \equiv 0$.

Most PDE-based restoration models, including the TV (4), the ITV (6), the Perona-Malik model[25], and the motion by mean curvature, can be formulated as

$$\frac{\partial u}{\partial t} + Su = Q(f-u), \tag{11}$$

where S is a (nonlinear) diffusion operator and Q denotes a nonnegative constraint term. Then it follows from (1) and (11) that the residual equation becomes

$$\frac{\partial v}{\partial t} + Qv = Su. \tag{12}$$

Thus, since $v(t=0)=0$, the residual at a positive time t_1, $v(t_1)$, remains zero in regions where $Su(t)=0$ for $0 \le t < t_1$, while it becomes nonzero elsewhere.

For the TV model (4), for example, the residual equation reads

$$\frac{\partial v}{\partial t} + \lambda u = -\nabla \cdot \left(\frac{\nabla u}{|\nabla u|} \right). \tag{13}$$

One can see from (13) that the residual of the TV model
becomes positive or negative at pixels where the image is
concave down or concave up, respectively. Thus the solution u of the TV model must involve nonphysical dissipation wherever its curvature is nonzero. Furthermore, we can see that the TV model (4) diffuses the image more actively as the local values of the curvature become larger in modulus. The above observation for the TV model can apply to general images and to the general model (11) as well:

The bigger the diffusion magnitude $|Su|$ is, the larger nonphysical dissipation the model (11) can insinuate into the restored image u.

This is an undesirable property for restoration models and also the major source of nonphysical dissipation for PDE-based restoration models to lose fine structures.

Ⅳ. EQUALIZED NET DIFFUSION (END)

This section begins with the introduction of the equalized net diffusion (END) modeling, which can yield a significant reduction of nonphysical dissipation near fine structures. Then, a linearized numerical procedure is suggested to solve the resulting models efficiently.

4.1. The END modeling

Recall that the ITV model (6) has been derived by scaling the TV model (4) by $|\nabla u|$ in order to suppress staircasing. Such a scaling idea can be applied further for the reduction of nonphysical dissipation. For example, as a scaling of (11), consider the following differential equation:

$$\frac{\partial u}{\partial t} + F(Su)Su = F(Su)Q(f-u), \tag{14}$$

where F is a positive scaling function. Then the stationary state of (14) must be the same as that of (11). In the following, we will select appropriate functions for F; the selected F in the right side may differ from that in the left side in order to optimize the reduction of nonphysical dissipation in image denoising.

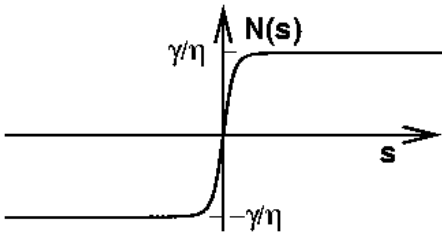

Fig. 1. The net diffusion function $N(s)$ in (17) for some choices of η and γ.

In order to get insights for an appropriate scaling

function, consider the following differential equation of the form

$$\frac{\partial u}{\partial t} + N(s) = R(f-u), \quad s = Su \qquad (15)$$

where N is a function of the diffusion Su and R denotes a nonnegative constraint function. In this article, we will call N the *net diffusion* (ND) function. Associated with (15), the residual equation reads

$$\frac{\partial v}{\partial t} + Rv = N(s)\ , \qquad (16)$$

We are interested in an ND function which does not introduce an excessive nonphysical dissipation near fine structures. Let us consider the following desirable properties of N:

(P1). *Increasing function of* s: The ND function N must be increasing, because otherwise the noise may not be effectively removed. For the model (15), image denoising occurs in practice along with both $|s|$ and $|N(s)|$ approaching zero.

(P2). *Origin-symmetry*: The origin-symmetry of N implies that $N(-s) = -N(s)$, with which N becomes equally diffusive for both concavities (up and down).

(P3). *Differentiability*: The ND function does not have to be smooth; however, a rough function may result in a coarse surface in the restored image.

(P4). *Boundedness and little variation*: We will choose N to be bounded and vary little over a wide range of $|s| \geq s_0 > 0$, for some s_0. As one can see from the residual equation (16), this property will set a net diffusion that is bounded and similar in large neighborhoods of fine structures. With such a "*diffusion equalization*" property, the residual may not be excessive on fine structures.

Let N satisfy the above properties, in particular (P4). Then we can set R to be independent of s or to be a constant. In a view point from the residual equation (16), such a setting must result in an equalized residual over a wide range of s and therefore over a wide range of frequency components in the image.

Now, we are ready to introduce an ND function N which satisfies all of the above properties:

$$N(s) = \frac{\gamma}{1+\eta|s|}s, \qquad (17)$$

where η and γ are positive constants to be selected appropriately. It is easy to see that N is increasing, origin-symmetric, differentiable, and bounded as follows: for all s,

$$|N(s)| \leq \frac{\gamma}{\eta}.$$

See Figure 1 for the ND function N with a certain choices of η and γ. It is not difficult to see that for a fixed s, $|s| > 0$, $N(s)$ approaches $\pm\gamma/\eta$, as η grows. Thus, for a large η (and γ), we have $|N(s)| \approx \gamma/\eta$ for a wide range of $|s| > 0$.

The ND function suggested in (17) has been motivated from an effort to find a variable parameter for the TV model (4). As an alternative to (5), one can get a variable parameter $\lambda = \lambda(\mathbf{x})$ by averaging *locally*:

$$\lambda = -\frac{1}{\sigma_{\mathbf{x}}^2}\frac{1}{|\Omega_{\mathbf{x}}|}\int_{\Omega_{\mathbf{x}}}(f-u)\kappa(u)\,d\mathbf{x}\,.$$

where $\Omega_{\mathbf{x}}$ is a neighborhood of $\mathbf{x}$ and $\sigma_{\mathbf{x}}^2$ denotes the local noise variance measured over $\mathbf{x}$. Then, the right side of the above equation can be approximated as

$$\lambda_{\mathbf{x}} \approx \frac{1}{\sigma_{\mathbf{x}}}\|f-u\|_{\mathbf{x}} \cdot \|\kappa(u)\|_{\mathbf{x}}, \qquad (18)$$

where $\|\cdot\|_{\mathbf{x}}$ denotes a local average over $\mathbf{x}$. Thus the TV model (4), when its stationary equation is scaled by $1/\|\kappa(u)\|_{\mathbf{x}}$ and regularized by a constant $\varepsilon_0 > 0$, can be rewritten as

$$\frac{\partial u}{\partial t} - \frac{1}{\|\kappa(u)\|_{\mathbf{x}}+\varepsilon_0}\kappa(u) = \frac{1}{\sigma_{\mathbf{x}}^2}\|f-u\|_{\mathbf{x}}(f-u), \qquad (19)$$

It is clear to see that the net diffusion of the above model is in the form of (17). The suggested ND function (17) is our choice of function which satisfies all the desirable properties (P1)~(P4); it will

be interesting to find more effective ND function.

The equation (15) will be called an equalized net diffusion (END)-incorporated model when it involves the ND function in (17):

$$\frac{\partial u}{\partial t}+\frac{\gamma}{1+\eta|Ss|}Su=\beta(f-u). \quad \text{(END)} \quad (20)$$

where Su is a diffusion operator and β is a function of $(\mathbf{x},t)$. For the selection of η and γ, see (26) and (27) below.

Note that the END function N in (17) also satisfies the
following property:

$$N(s)\approx\gamma s, \text{ for } s \text{ small},$$

which implies that in smooth regions, the END-incorporated model (20) behaves similar (up to a scalar factor) to the basic restoration model (11).

Remark. A closely related work to (20) can be found from [8]. There the authors have suggested a time-stepping numerical procedure called the *method of nonflat time evolution* (MONTE), in which the timestep size is determined based on local image characteristics such as the curvature or the diffusion magnitude, in order to significantly reduce nonphysical dissipation and preserve fine structures satisfactorily. The END modeling shares mathematical foundations and applicability with the MONTE procedure. A considerable difference (in its numerical realization) comes from the choice of the constraint term. Performances of these two techniques will be compared and appear elsewhere along with mathematical analyses that address significance, roles, and various choices of the diffusion and constraint terms in diverse PDE-based image processing tasks[5].

4.2. A linearized time-stepping procedure

In this subsection, we introduce an efficient time-stepping procedure for the END-incorporated model (20). Let Δt be the timestep size and $t^n=n\Delta t,\ n\geq 0$. Define $u^n=(\cdot\,,t^n)$. For a simpler presentation, we will exemplify the diffusion operator of the ITV model, i.e.,

$$Su=-|\nabla u|\,\nabla\cdot\left(\frac{\nabla u}{|\nabla u|}\right). \quad (21)$$

For $\ell=1,\,2$ and $m=n,\,n-1$, let

$$S_\ell^{n-1}u^m=-|\nabla_h u^{n-1}|\,D_{x_\ell}\left(\frac{D_{x_\ell}u^m}{|\nabla_h u^{n-1}|}\right), \quad (22)$$

where $(D_{x_1},D_{x_2})^T$ is the half-step central difference operator for the gradient ∇ and $|\nabla_h u^{n-1}|$ denotes a numerical approximation of gradient magnitude $|\nabla u^{n-1}|$ such as the (standard) second-order central scheme. Letting $S^{n-1}=S_1^{n-1}+S_2^{n-1}$, we define

$$A_\ell^{n-1}:=\frac{\gamma}{1+\eta|S^{n-1}u^{n-1}|}S_\ell^{n-1}+\frac{\beta^{n-1}}{2}. \quad (23)$$

Note that A_ℓ^{n-1}, $\ell=1,\,2$, are tri-diagonal matrices. Set $A^{n-1}=A_1^{n-1}+A_2^{n-1}$. Then, an *incomplete* (linearized) Crank-Nicolson scheme for (20) reads

$$\frac{u^n-u^{n-1}}{\Delta t}+A^{n-1}\frac{u^n+u^{n-1}}{2}\beta^{n-1}f. \quad (24)$$

One can solve the linear system (24) by applying an iterative algebraic solver. However, for an efficiency reason, we employ the *alternating direction implicit* (ADI) time-stepping procedure [11], [12] for (24):

$$\begin{aligned}\left(I+\frac{\Delta t}{2}A_1^{n-1}\right)u^*&=\left(I-\frac{\Delta t}{2}A_1^{n-1}-\Delta tA_2^{n-1}\right)u^{n-1}\\&\quad+\Delta t\beta^{n-1}f,\\ \left(I+\frac{\Delta t}{2}A_2^{n-1}\right)u^n&=u^*+\frac{\Delta t}{2}A_2^{n-1}u^{n-1},\end{aligned} \quad (25)$$

where u^* is an intermediate solution and I denotes the identity matrix. We will call (25) the Crank-Nicolson ADI (CN-ADI) algorithm.

V. CHOICES FOR η AND γ

For the END-incorporated model (20), we have

introduced two extra parameters: η and γ. In this section, we present a guideline for the automatic choice of these two parameters. In order to carry out a systematic analysis, we have selected a group of images, which are scaled to have values between 0 and 1 for all numerical experiments. The parameter choices hereafter in this article is based on such a scaling and the use of CN-ADI (25).

Each of selected images is perturbed by Gaussian noise of various levels; each of noisy images has been denoised many times, with diverse choices of the parameters, to find the best restored image. From the experiment, a useful relationship between η and γ has been found; we may determine the parameter γ^n (on each time level) in such a way that for given η, the arithmetic average of $\gamma/(1+\eta|s^n|)$ becomes 1 over the whole domain, i.e.,

$$\gamma^n = N_x N_y \left(\sum_{i=1}^{N_x} \sum_{j=1}^{N_y} \frac{1}{1+\eta|s_{ij}^n|} \right)^{-1} \qquad (26)$$

where N_x and N_y denote the number of pixels in the image in the horizontal and vertical directions, respectively. As we have observed earlier, η must be large enough (when γ/η is fixed or (26) holds) to equalize the net diffusion over a wide range of the diffusion $s(=Su)$. However, it cannot be set too large. In particular, when the observed image has a high noise level and the desired image is relatively smooth, most high frequency components in the image must come from
the noise. In the case, it can be better to allow the END-incorporated model to diffuse higher frequency components more actively by setting the parameter η smaller. We will consider a strategy for the choice of η for relatively smooth images as shown in Figure 2.

Let S_0 be the arithmetic average of the absolute diffusion of the noisy image $|Su^0| = |Sf|$. It has been found from the experiment that for the data set $\{S_0, \eta\}$ obtained from the same image with different noise levels, $\log\eta$ reveals a linear dependence on $\log(S_0)$, as shown in Figure 3. A regression analysis is applied, for the model

$$\log\eta = c_1 + c_2 \log(S_0).$$

to found $c_1 = 1.037$ and $c_2 = -2.460$. Thus one can choose η as follows:

$$\eta = 2.82 \cdot S_0^{-2.46}. \qquad (27)$$

With the aforementioned scaling, i.e., $f \in [0,1]$, the average diffusion S_0 turns out to have values between 0.1 and 0.7 for most images of small to reasonable noise levels. This implies that for most cases, η can be selected between 6.78 and 813, with its value becoming smaller for larger S_0. The strategy in (27) has been developed for relatively smooth images. For texture images, the parameters must be chosen larger as the texture becomes more delicate. Unfortunately, we could not find any useful patterns from the data of parameters which produce best restored images. Only the useful guideline is that the best performing η can be chosen between 30 and 2000, with the parameter being near 2000 for lower noise levels.

VI. NUMERICAL EXPERIMENTS

In this section, we present numerical results and show

effectiveness of the END modeling (20) by comparing the *peak signal-to-noise ratio* (PSNR) for the following four models: ITV (6), NC (7), END-incorporated ITV (E-ITV), and END-incorporated NC (E-NC). The parameter γ is chosen as in (26) for all cases. For the choice of parameter η, we apply the strategy in (27) for relatively smooth images; for texture images, the choices of η will be indicated in figure captions. The constraint term β is set dynamically utilizing the method of texture-free residual parameterization[15].

6.1. Relatively smooth images

In Table 1, we present a PSNR analysis for the relatively smooth images in Figure 2. For each of

the images, PSNRs are presented for a noisy image f and recovered images by four different models, as a distance from the original image. The integers in the parentheses indicate the number of CN-ADI iterations to reach the best restored image measured in PSNR. As one can see from the table, the END-incorporated models (E-ITV and E-NC) outperform the basic models (ITV and NC), while the NC diffusion models (NC and E-NC) improve the image quality over ITV-related models. Thus the E-NC model performs the best for all cases. Here it should be noticed that the NC model tends to take more iterations to reach its best image than the ITV model. However, this does not imply that the NC diffusion makes the denoising procedure slow down. For example, for the Fireworks image, four iterations of the NC model obtains an image of PSNR=29.9, which is much larger than that of the ITV model (26.5). It is safe to say that the NC diffusion just runs more steps to improve image quality in higher levels. The improvement by the END modeling looks less effective for the NC model than the ITV model. For example, for Fireworks, the END modeling makes the ITV model improve from 26.5 to 30.8 in PSNR, while it drives the NC model from 29.9 to 31.9. However, it does not mean that the END modeling may be ineffective for some basic models. It is simply because the NC model itself is able to produce images much better than the ITV model and as one can see from the table, the E-NC model restores images of similar (slightly better) qualities as the E-ITV model. One also should notice that the END-incorporated models produce their best restored images in 3-5 iterations. In particular, the E-NC model has never taken more than four iterations for all examples we have tested, including texture images to be presented in the next subsection. The END modeling improves not only image quality but also computational efficiency.

Figure 4 shows performances of the four restoration models applied to one of sample images in Figure 2, Chess. The original image in Figure 4(a) is contaminated by a Gaussian noise of PSNR=24.0 as in Figure 4(b). The END-incorporated models have introduced considerable improvements over both ITV and NC (compared from visual content); see Table 1 for a PSNR comparison. In particular, as one can see from Figure 4(a) and Figure 4(f), the E-NC model can preserve and restore image details very successfully without introducing an observable blur, just in three CN-ADI iterations.

6.2. Texture images

For texture images, we select Train and Zebra from public domain.

Figure 5 contains numerical results for a Train image. The original image in Figure 5(a) is perturbed by a Gaussian noise of PSNR=24.3, as in Figure 5(b), and restored by the four models. The PSNRs (and iteration counts) for the restored images in Figures 5(c)-5(f) are respectively 23.2 (2), 25.3 (11), 26.7 (3), and 27.0 (3). The iterates of the ITV model show PSNRs continuously decreasing as the iteration count grows; we just stopped in two iterations to get an image. As for relatively smooth

Fig. 2. Sample images utilized for the analysis of an automatic choice of the parameter η: (left to right and top to bottom) Bamboo, Chess, Elaine, Fireworks, Flowers, House, Lenna, and Ring.

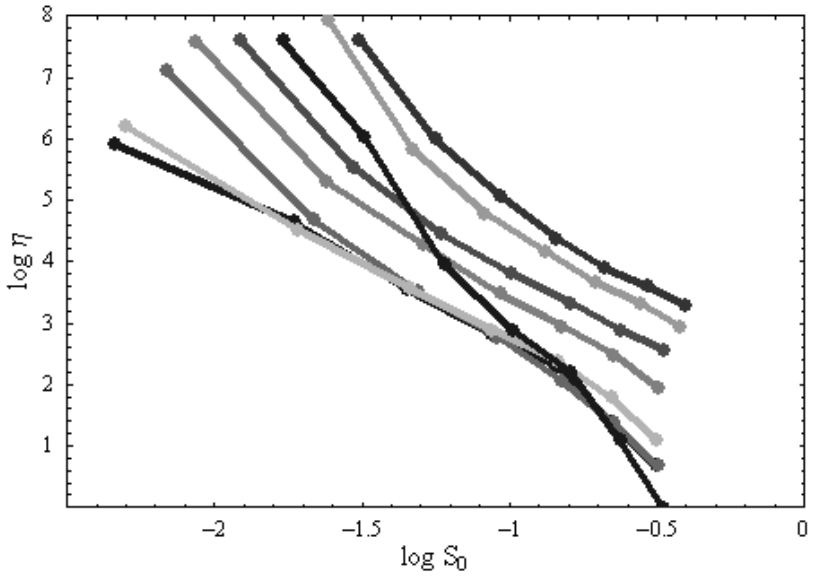

Fig. 3. The log-log plot for S_0 and η which produce the best restored images. The data points obtained from the same image (with different noise levels) are connected by line segments to show the linearity between $\log S_0$ and $\log \eta$.

Table. 1. A PSNR analysis for relatively smooth images. The integers in the parentheses indicate the number of CN-ADI iterations to reach the best restored image.

	f	ITV	NC	E-ITV	E-NC
Bamboo	23.8	33.5 (8)	34.7 (5)	34.1 (5)	34.9 (3)
Chess	24.0	27.3 (5)	30.0 (4)	30.0 (4)	30.7 (3)
Elaine	25.2	33.3 (3)	33.6 (3)	33.7 (3)	33.7 (3)
Fireworks	26.3	26.5 (4)	29.9 (15)	30.8 (4)	31.9 (3)
Flowers	25.0	28.1 (3)	31.1 (8)	31.1 (5)	31.9 (3)
House	26.1	34.0 (5)	35.2 (4)	35.1 (4)	35.4 (3)
Lenna	29.6	32.8 (2)	35.6 (10)	35.7 (3)	36.3 (3)
Ring	27.4	33.5 (5)	36.4 (15)	35.9 (5)	37.0 (3)

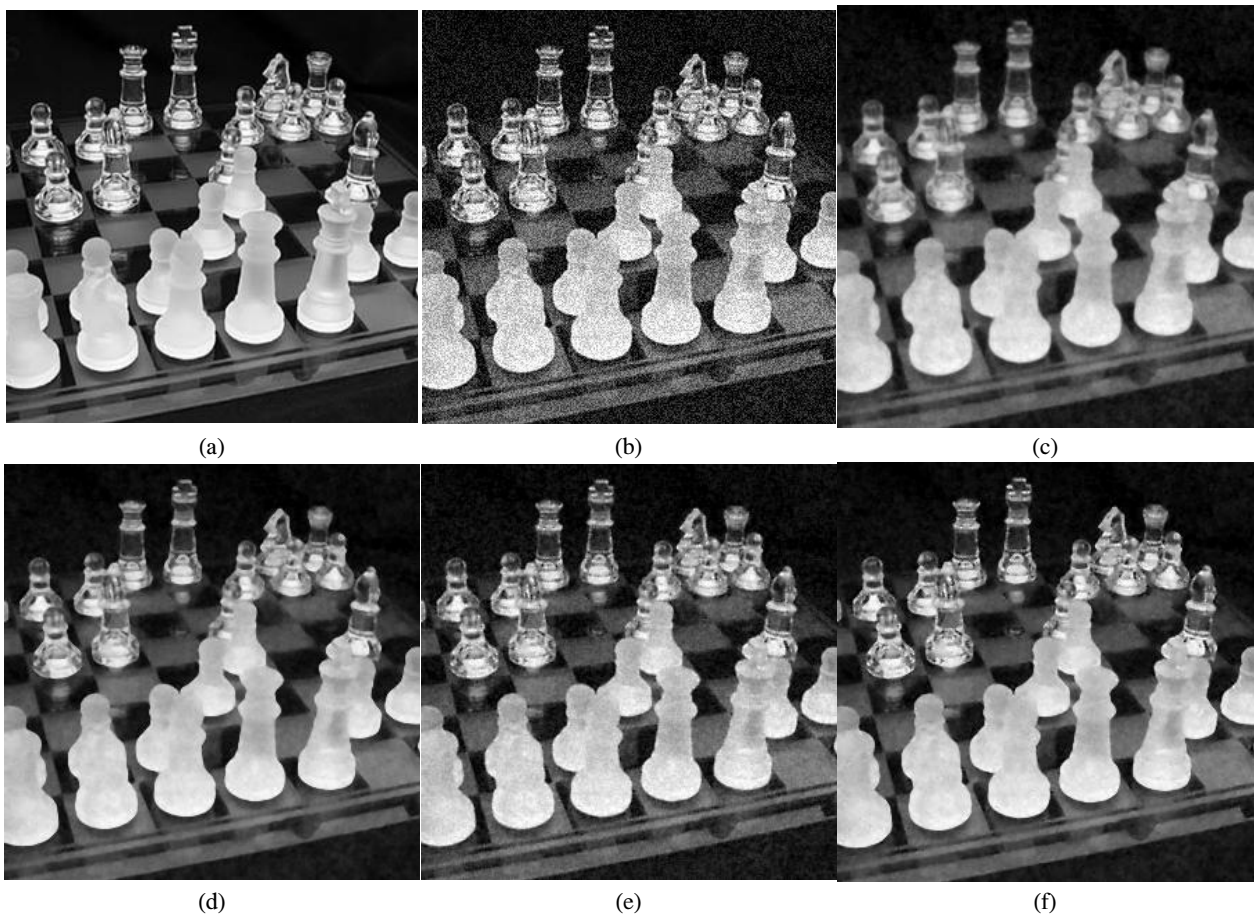

Fig. 4. Chess: (a) The original image, (b) a noisy image contaminated by a Gaussian noise (PSNR=24.0), and restored images by (c) ITV, (d) NC, (e) E-ITV, and (f) E-NC.

images, the END-incorporated models have improved both image quality and computationally efficiency; they can preserve and restore the texture image satisfactorily in three CN-ADI iterations.

In Figure 6, in order to make a systematic comparison of the four models, we present the magnified residuals $3(g-u)+128$, where g is the original image in Figure 5(a) and u is a restored image in Figures 5(c)-5(f). It is apparent that the basic models lose fine structures during the image restoration. On the other hand, the residuals from the END-incorporated models are much less structural.

In Figure 7, we show numerical results for a Zebra image in the same manner as in Figure 5. The noisy image contains a Gaussian noise of PSNR=24.8. The PSNRs (and iteration counts) in Figures 7(c)-7(f) are respectively 24.1 (5), 27.3 (5), 28.9 (4), and 29.8 (3).We have observed magnified residuals to reach the same conclusion for the END-incorporated models as in the previous example. Compare Figure 7(f) with Figure 7(a); the E-NC model can restore fine structures in the texture image satisfactorily and efficiently.

In order to further investigate effectiveness of the END modeling, Figure 8 presents images of Zebra head each of which is taken from bottom left of the images in Figure 7. The images are in 150×100 pixels and depicted without applying scaling of the word processing software. As one might be expected, the restored images by the basic models (ITV and NC) have lost fine structures to look blurry as shown in Figures 8(c) and 8(d). The E-ITV model restores an image of reasonably well-preserved fine structures, while it has a certain degree of noise left to the final image, Figures 8(e).

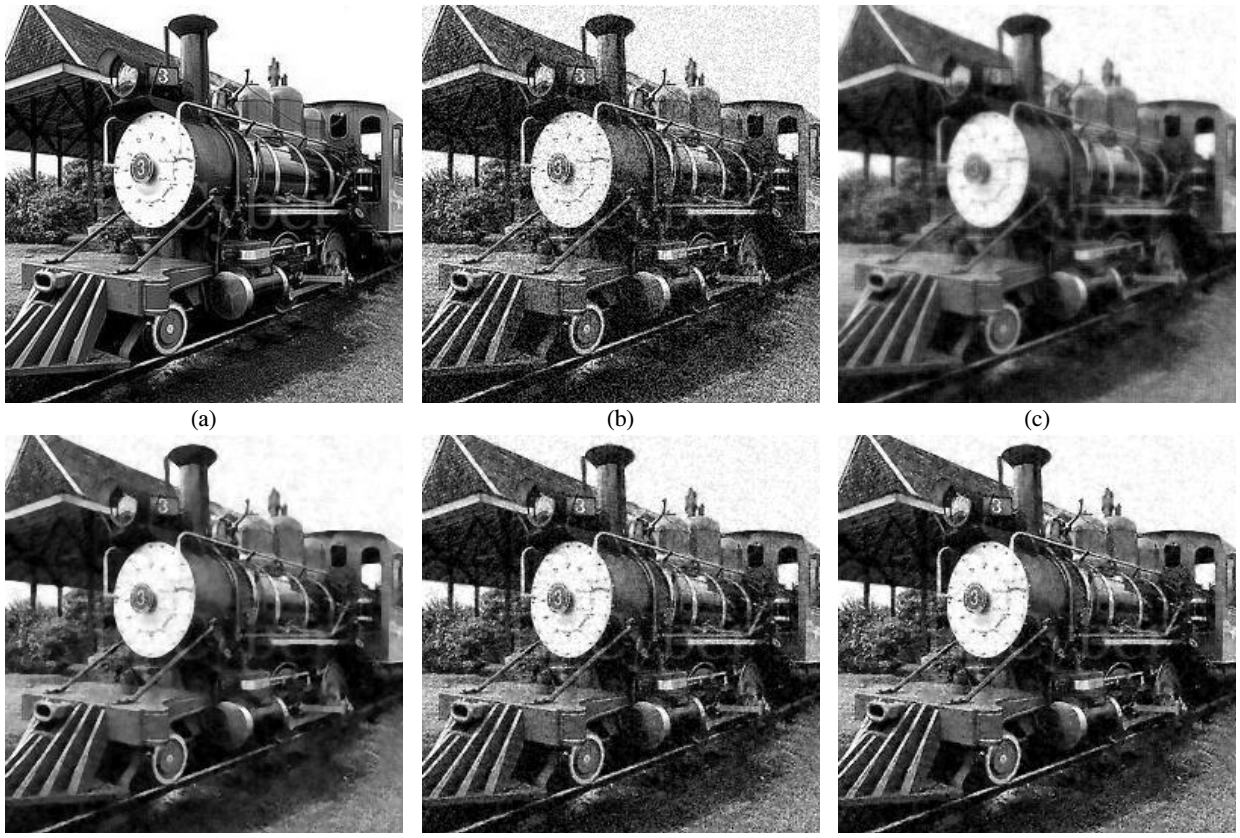

(a) (b) (c)

(d) (e) (f)

Fig. 5. Train: (a) The original image, (b) a noisy image contaminated by a Gaussian noise (PSNR=24.3), and restored images by (c) ITV, (d) NC, (e) E-ITV, and (f) E-NC. Set $\eta = 50$.

On the other hand, the E-NC model is able to remove noise effectively preserving fine structures most satisfactorily. Look at the (back) ground in particular. There is no doubt that the E-NC model can achieve the largest PSNR value.

Ⅶ. CONCLUSIONS

This article suggests a mathematical technique which modifies PDE-based restoration models to effectively control nonphysical dissipation. PDE-based models have a tendency of losing fine structures. We have analyzed sources of such an undesirable loss and have introduced the so-called equalized net diffusion (END) modeling, as a modification technique of basic PDE-based models. A linearized Crank-Nicolson alternating direction implicit (CN-ADI) numerical procedure has been applied to compute

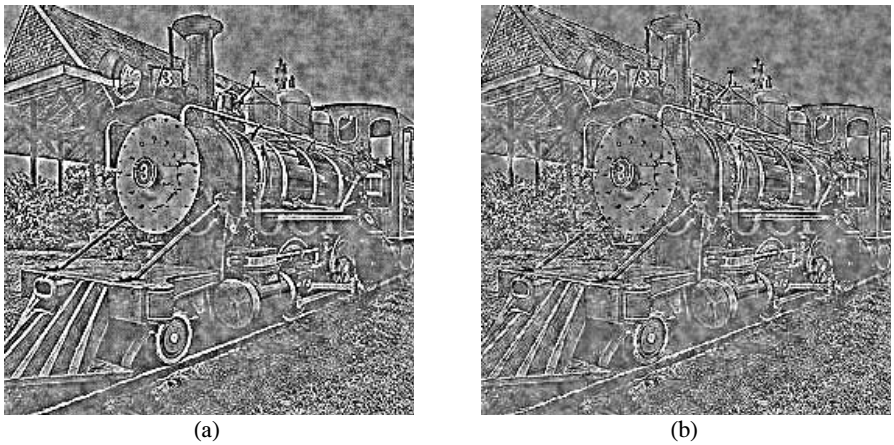

(a) (b)

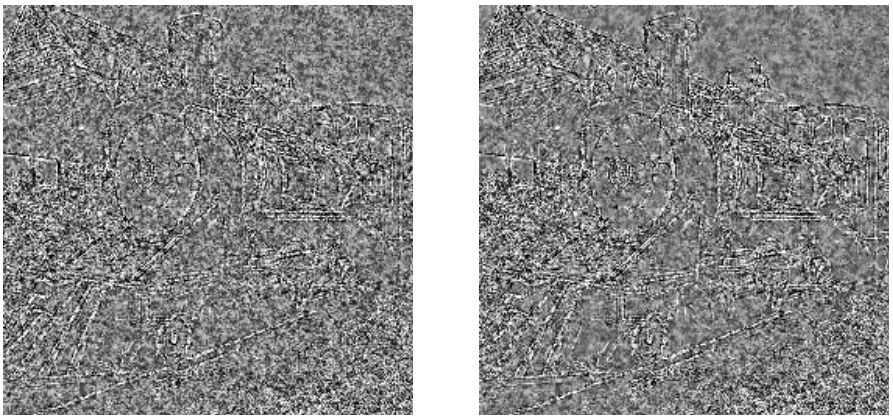

(c) (d)

Fig. 6. Magnified residuals $3(g-u)+128$, where g is the original image in Figure 5(a) and u is the restored image by (a) ITV, (b) NC, (c) E-ITV, and (d) E-NC.

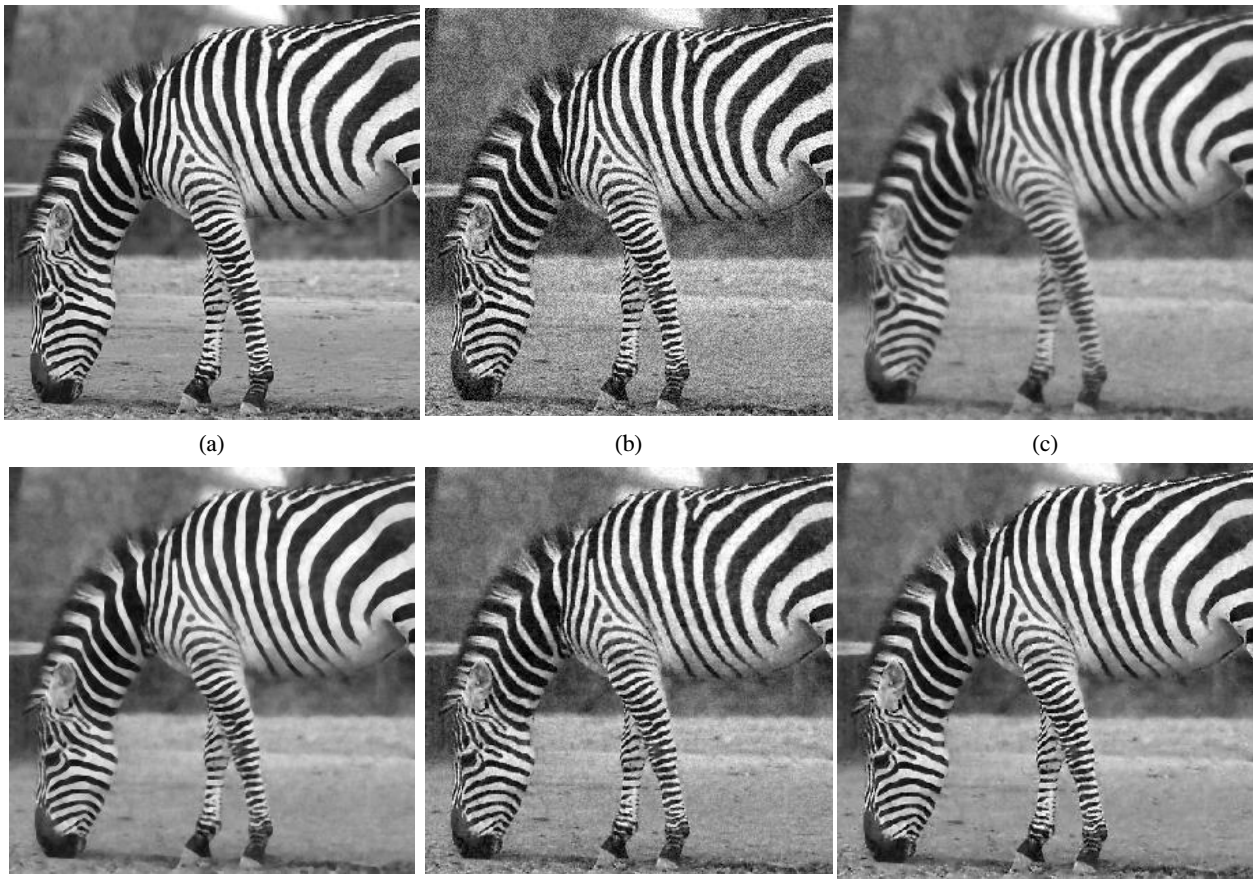

(a) (b) (c)

(d) (e) (f)

Fig. 7. Zebra: (a) The original image, (b) a noisy image contaminated by a Gaussian noise (PSNR=24.8), and restored images by (c) ITV, (d) NC, (e) E-ITV, and (f) E-NC. Set $\eta = 40$.

Fig. 8. Zebra head in 150×100 pixels, taken from Figure 7: (a) The original image, (b) a noisy image contaminated by a Gaussian noise (PSNR=24.8), and restored images by (c) ITV, (d) NC, (e) E-ITV, and (f) E-NC.

the END-incorporated models efficiently. The parameters introduced in the END modeling have been analyzed for relatively smooth images. It has been numerically verified that END-incorporated models can restore fine structures satisfactorily in 3-5 CN-ADI iterations. The END modeling has been proved to improve not only image quality but also computational efficiency, over basic PDE based restoration models.

REFERENCES

[1] L. Alvarez, P. Lions, and M. Morel, "Image selective smoothing and edge detection by nonlinear diffusion. II," *SIAM J. Numerical Anal.*, vol. 29, no. 3, pp. 845-866, June 1992.

[2] G. Aubert and P. Kornprobst, *Mathematical Problems in Image Processing*, *Series: Applied Math. Sci.*, vol. 147, Springer-Verlag, 2002.

[3] P. V. Blomgren and T. F. Chan, "Color TV: Total variation methods for restoration of vector valued images," *IEEE Trans. Image Process.*, vol. 7, no. 3, pp. 304-309, Mar. 1998.

[4] F. Catte, P. Lions, M. Morel, and T. Coll, "Image selective smoothing and edge detection by nonlinear diffusion," *SIAM J. Numerical Anal.*, vol. 29, no. 3, pp. 182-193, June 1992.

[5] Y. Cha and S. Kim, "Diffusion and constraint terms in PDE-based image restoration, zooming, deconvolution, and segmentation," *in preparation*.

[6] Y. Cha and S. Kim, "Edge-forming methods for color image zooming," *IEEE Trans. Image Process.*, vol. 15, no. 8, pp. 2315-2323, Aug. 2006.

[7] Y. Cha and S. Kim, "Edge-forming methods for image zooming," *J. Math. Imaging Vision*, vol. 25, no. 3, pp. 353-364, Oct. 2006.

[8] Y. Cha and S. Kim, "The method of nonflat time evolution (MONTE) in PDE-based image restoration," *J. Korea Inform. Commun. Soc. (KICS)*, vol. 37A, no. 11, pp. 961-971, Nov. 2012.

[9] T. Chan, S. Osher, and J. Shen, "The digital

TV filter and nonlinear denoising," *IEEE Trans. Image Process.*, vol. 10, no. 2, pp. 231-241, Feb. 2001.

[10] T. F. Chan and J. Shen, "Variational restoration of non-flat image features: Models and algorithms," *SIAM J. Appl. Math.*, vol. 61, no. 4, pp. 1338-1361, Jan. 2001.

[11] J. Douglas, Jr. and J. Gunn, "A general formulation of alternating direction methods Part I. Parabolic and hyperbolic problems," *Numerical Math.*, vol. 6, no. 1, pp. 428-453, Dec. 1964.

[12] J. Douglas, Jr. and S. Kim, "Improved accuracy for locally one-dimensional methods for parabolic equations," *Math. Models Methods Appl. Sci.*, vol. 11, no. 9, pp. 1563-1579, Dec. 2001.

[13] R. Gonzalez and R. Woods, *Digital Image Processing*, 2nd Ed., Prentice-Hall, 2002.

[14] S. Kim, "Equalized net diffusion (END) in image denoising," in *Proc. 10th WSEAS Int. Conf. Appl. Math.*, pp. 349-354, Istanbul, Turkey, May 2006.

[15] S. Kim, "PDE-based image restoration: A hybrid model and color image denoising," *IEEE Trans. Image Process.*, vol. 15, no. 5, pp. 1163-1170, May 2006.

[16] S. Kim and H. Lim, "A non-convex diffusion model for simultaneous image denoising and edge enhancement," *Electron. J. Differential Equations (EJDE)*, Conference Special Issue, vol. 15, pp. 175-192, Feb. 2007.

[17] R. Kimmel and N. Sochen, "Orientation diffusion or how to comb a porcupine?" *J. Visual Commun. Image Representation*, vol. 13, no. 1-2, pp. 238-248, Mar. 2002.

[18] A. Marquina and S. Osher, "Explicit algorithms for a new time dependent model based on level set motion for nonlinear deblurring and noise removal," *SIAM J. Sci. Comput.*, vol. 22, no. 2, pp. 387-405, Aug. 2000.

[19] Y. Meyer, *Oscillating Patterns in Image Processing and Nonlinear Evolution Equations*, *Series: University Lecture Series*, vol. 22, American Mathematical Society, 2001.

[20] S. Mitra and G. Sicuranza, *Nonlinear Image Processing*, Academic Press, 2001.

[21] J.-M. Morel and S. Solimini, *Variational Methods in Image Segmentation*, *Series: Progress in Nonlinear Differential Equations and Their Applications*, vol. 14, Birkhäuser, 1995.

[22] M. Nitzberg and T. Shiota, "Nonlinear image filtering with edge and corner enhancement," *IEEE Trans. Pattern Anal. Mach. Intell.*, vol. 14, no. 8, pp. 826-833, Aug. 1992.

[23] S. Osher, M. Burger, D. Goldfarb, J. Xu, and W. Yin, "Using geometry and iterated refinement for inverse problems (1): Total variation based image restoration," *CORC Technical Report 2004-03*, Mar. 2004.

[24] S. Osher and R. Fedkiw, *Level Set Methods and Dynamic Implicit Surfaces*, Springer-Verlag, 2003.

[25] P. Perona and J. Malik, "Scale-space and edge detection using anisotropic diffusion," *IEEE Trans. Pattern Anal. Mach. Intell.*, vol. 12, no. 7, pp. 629-639, July 1990.

[26] L. Rudin, S. Osher, and E. Fatemi, "Nonlinear total variation based noise removal algorithms," *Physica D: Nonlinear Phenomena*, vol. 60, no. 1-4, pp. 259-268, Nov. 1992.

[27] G. Sapiro, *Geometric partial differential equations and image analysis*, Cambridge University Press, 2001.

[28] N. Sochen, R. Kimmel, and R. Malladi, "A general framework for low level vision," *IEEE Trans. Image Process.*, vol. 7, no. 3, pp. 310-318, Mar. 1998.

[29] R. Weinstock, *Calculus of Variations*, Dover Pubilcations, 1974.

[30] Y.-L. You, W. Xu, A. Tannenbaum, and M. Kaveh, "Behavioral analysis of anisotropic diffusion in image processing," *IEEE Trans. Image Process.*, vol. 5, no. 11, pp. 1539-1553, Nov. 1996.

Youngjoon Cha

Professor, Department of Applied Mathematics, Sejong University

1988, B.S., Department of Mathematics, Seoul National University

1990, M.S., Department of Mathematics, Seoul National University

1997, Ph.D., Department of Mathematics, Purdue University

<Research Interests> Image Processing & Computer Vision, Epidemiology, Wave Simulation

Seongjai Kim

Associate Professor, Department of Mathematics and Statistics, Mississippi State University

1988, B.S., Department of Mathematics, Seoul National University.

1990, M.S., Department of Mathematics, Seoul National University.

1995, Ph.D., Department of Mathematics, Purdue University.

<Research Interests> Image Processing & Computer Vision, Computational seismology, Wave Simulation